Structure and variability of the shelfbreak East Greenland Current north of Denmark Strait

L. Håvik* and K. Våge

Geophysical Institute, University of Bergen and Bjerknes Centre for Climate Research, Bergen, Norway

R. S. Pickart and B. Harden

Woods Hole Oceanographic Institution, Woods Hole, USA

W.-J. von Appen

Alfred Wegener Institute, Helmholtz Centre for Polar and Marine Research, Bremerhaven, Germany

S. Jónsson

Marine and Freshwater Research Institute, Reykjavik and University of Akureyri, Akureyri, Iceland

S. Østerhus

Uni Research Climate, Bjerknes Centre for Climate Research, Bergen, Norway

in preparation for

Journal of Physical Oceanography

Generated using v4.3.2 of the AMS LaTeX template

Corresponding author address: L. Håvik, Geophysical Institute, University of Bergen and Bjerknes Centre for Climate Research, Bergen, Norway

E-mail: lisbeth.havik@uib.no

ABSTRACT

Data from a mooring array deployed north of Denmark Strait from September 2011 to August 2012 are used to investigate the structure and variability of the shelfbreak East Greenland Current (EGC). The shelfbreak EGC is a surface-intensified current situated just offshore of the east Greenland shelfbreak flowing southward through Denmark Strait. We identified two dominant spatial modes of variability within the current: a pulsing mode and a meandering mode, both of which were most pronounced in fall and winter. A particularly energetic event in November 2011 was related to a reversal of the current for nearly a month. In addition to the seasonal signal, the current was associated with periods of enhanced eddy kinetic energy and increased variability on shorter timescales. Our data indicate that the current is, for the most part, barotropically stable but subject to baroclinic instability from September to March. By contrast, in summer the current is mainly confined to the shelfbreak with decreased eddy kinetic energy and minimal baroclinic conversion. No other region of the Nordic Seas displays higher levels of eddy kinetic energy than the shelfbreak EGC north of Denmark Strait during fall. This appears to be due to the large velocity variability on mesoscale timescales generated by the instabilities. The mesoscale variability documented here may be a source of the variability observed at the Denmark Strait sill.

1. Introduction

The East Greenland Current (EGC) provides a direct connection between the Arctic Ocean and the North Atlantic and is the main export pathway for both solid and liquid freshwater from the Arctic Ocean (Dickson et al. 2007). In addition to the freshwater transport, dense water masses formed in the Nordic Seas and the Arctic Ocean are carried south by the EGC toward Denmark Strait. Since the intermediate and deep water masses in the EGC are denser than the ambient water in the North Atlantic, they sink toward the deep ocean as an overflow plume after crossing the Denmark Strait sill. This overflow plume from the Nordic Seas contributes to the deep limb of the Atlantic Meridional Overturning Circulation. Roughly half of the total dense overflow across the Greenland-Scotland Ridge exits through Denmark Strait (Dickson et al. 2008). Hence, Denmark Strait is a key location for the exchange and coupling between the Arctic Ocean, the Nordic Seas, and the North Atlantic Ocean.

North of Denmark Strait the circulation that supplies the freshwater and dense overflow water to the North Atlantic is complex and variable. As the EGC approaches Denmark Strait, it bifurcates into two branches: the shelfbreak EGC and the separated EGC (Våge et al. 2013) (Fig. 1), with the latter flowing along the base of the Iceland continental slope toward the strait. Våge et al. (2013) proposed two different mechanisms that may be responsible for the formation of the separated EGC. Using a simplified model they argued that eddies shed from the shelfbreak EGC at the northern end of the Blosseville Basin migrate offshore toward the Iceland slope where they coalesce and form a coherent current. The other mechanism is associated with negative wind stress curl over the Blosseville Basin. Closed f/h contours within the basin could lead to an anti-cyclonic circulation whose eastern branch is the separated EGC. The observations used by Våge et al. (2013) came from only four summertime shipboard occupations of the Kögur transect between the Iceland and Greenland shelves across the Blosseville Basin (Fig. 1). Year-long time-series from a mooring array deployed along the same transect confirmed the existence of the two EGC branches, and Harden et al. (2016) found that the partitioning of transport between the two branches varied on a weekly timescale due to wind forcing.

Recently, Håvik et al. (2017) identified a third component of the boundary current system approaching Denmark Strait: the Polar Surface Water Jet (Fig. 1). This current is situated on the east Greenland shelf, onshore of the shelfbreak branch, and accounts for a sizeable fraction of the total southward freshwater transport of the EGC system (up to 55% in their sections). In addition to the branches of the EGC, the North Icelandic Jet (NIJ) transports overflow water toward Denmark Strait along the Iceland continental slope (Jónsson 1999; Jónsson and Valdimarsson 2004; Våge et al. 2011). This current is hypothesized to be the lower limb of a local overturning cell in the Iceland Sea whose upper limb is the North Icelandic Irminger Current (Våge et al. 2011). Unlike the EGC, the NIJ is not associated with any substantial freshwater transport (de Steur et al. 2017).

Jochumsen et al. (2012) estimated a mean transport of Denmark Strait Overflow Water (DSOW, $\sigma_\theta \geq 27.8$ kgm^{-3}) of 3.4 Sv at the Denmark Strait sill for the period 1996 to 2011, with no pronounced seasonal or inter-annual variability. However, on timescales of 2-10 days the velocities and corresponding transports exhibited pronounced variability. Smith (1976) identified oscillations in the flow through Denmark Strait on timescales of 2 days in current meter data, and attributed this variability to baroclinic instability of the overflow. Recently, two features have been identified as the dominant sources of mesoscale variability at the Denmark Strait sill: boluses and pulses (Mastropole et al. 2017; von Appen et al. 2017). The boluses are large lenses of weakly stratified overflow water associated with a modest strengthening of the flow. By contrast, pulses correspond to a strong increase in velocity when the overflow water is confined to a thin layer above the bottom. On average either of these features are present at the sill every second day.

Presently it is unclear whether the variability in Denmark Strait arises from local processes or if it is a result of upstream variability in the currents approaching the strait. Most of our knowledge of both the water masses and the kinematic structure of the EGC farther north, between Fram Strait and Denmark Strait, is based on analysis of synoptic summer sections (Rudels et al. 2002, 2005; Jeansson et al. 2008; Nilsson et al. 2008; Våge et al. 2013; Håvik et al. 2017). These studies generally found that the EGC is a surface-intensified current which closely follows the topography of the shelfbreak toward Denmark Strait. However, such snapshots do not elucidate the variability throughout the year. Due to the presence of pack ice, observations from the rest of the year have primarily been obtained by moorings.

Strass et al. (1993) analyzed a year-long data set from four moorings deployed across the EGC close to 75°N in 1987-1988. They showed that the current was highly variable on timescales of a few days, which they attributed to baroclinic instability. Furthermore, they found that this process varied seasonally, and that the necessary condition for baroclinic instability was not always fulfilled. Based on one year of mooring data across the EGC (also from 75°N, 1994-1995),Woodgate et al. (1999) found that the kinematic structure of the current changed significantly from month to month. While their transport timeseries clearly varied on timescales of days, their focus was on longer timescales and hence they did not elaborate on this. More recently, Harden et al. (2016) calculated the transport of DSOW across the Kögur transect from moored observations (Fig. 1). They estimated a total transport of DSOW ($\sigma_\theta \geq 27.8$ kgm^{-3}) of 3.54 ± 0.16 Sv, with the largest contribution from the shelfbreak EGC (1.50 ± 0.16 Sv). Consistent with the measurements farther north, both branches of the EGC, as well as the NIJ, varied substantially on timescales of a few days.

In order to explain this high frequency variability, it is necessary to understand the dynamics of the individual currents that flow into Denmark Strait. To address this we use year-long records of velocity and hydrography obtained from the mooring array deployed along the Kögur transect north of Denmark Strait (i.e. the same data set used by Harden et al. 2016). The moorings spanned the full width of the Blosseville Basin north of Denmark Strait and sampled the shelfbreak EGC, the separated EGC, and the NIJ (Fig. 1). The Polar Surface Water Jet on the Greenland shelf was not covered by the array. In this study we focus on the shelfbreak EGC which is the major pathway of DSOW to the sill and also supplies on average 70% of the freshwater transport in the EGC system to Denmark Strait (de Steur et al. 2017). Our primary goal is to obtain a robust description of the mean state and variability of this branch and shed light on the dynamics that govern its flow. This is essential for understanding the interaction between the currents in this region, such as the bifurcation of the EGC or the time-varying compensation between the two EGC branches described by Harden et al. (2016). Our data set provides a unique opportunity to examine the variability of the shelfbreak EGC throughout one year and how this in turn may influence both the flux of freshwater and dense overflow water toward the North Atlantic.

2. Data and methods

From September 2011 to August 2012 a densely instrumented mooring array was deployed along the Kögur transect north of Denmark Strait from the Iceland shelfbreak to the east Greenland shelfbreak (Fig. 1). The mooring array was designed to measure hydrographic properties and velocity in the shelfbreak EGC, the separated EGC, and the NIJ, and consisted of 12 moorings named KGA 1 – KGA 12. The depth-integrated current vectors over the top 500 m for the entire deployment period with corresponding standard error ellipses are shown in Fig. 2. The ellipses were estimated based on a calculated integral timescale of 6-9 days (Hogg et al. 1999).

Across the outer east Greenland shelf and slope the shelfbreak EGC closely followed the bathymetry and was on average directed toward the southwest at a maximum depth-integrated speed of 15 cms^{-1} at KGA 11. On the slope the standard error ellipses were elongated in the southwest-northeast direction, whereas at the moorings across the deeper part of the Blosseville Basin (KGA 7 – KGA 9) the error ellipses were more circular with a weaker mean velocity toward the southwest. This region of weaker flow in the interior basin differentiates the shelfbreak branch from the separated branch. Over the deep part of the Iceland slope the increased current velocities mark the presence of the separated EGC and the NIJ, both directed toward the southwest. On the upper Iceland slope the array measured the offshore edge of the northeastward-flowing North Icelandic Irminger Current.

Our focus is on the shelfbreak EGC, and in order to investigate this current branch we used data from the 5 northwesternmost moorings (KGA 8 – KGA 12 in Figs. 2 and 3). This subset of moorings extended from the outer east Greenland shelf to the interior of the Blosseville Basin. The moorings were equipped with recording current meters (RCMs), acoustic doppler current profilers (ADCPs) and temperature-conductivity-pressure sensors (Microcats) at different levels. In order to remove the tides and other high frequency variability, all measurements were low-pass filtered with a cut-off at 36 hours. For a detailed description of the data processing and measurement errors, the reader is referred to Harden et al. (2016).

We defined a coordinate system that was rotated 139° counter-clockwise from east such that the along-stream current direction (v) corresponded to the mean current direction at KGA 11 (indicated in lower left corner of Fig. 2). This was also the direction of maximum variance as seen by the error ellipses in Fig. 2. The cross-stream distance (x) is measured from the easternmost mooring and increases toward Greenland. Positive along-stream velocity (v) is toward the southwest and positive cross-stream velocity (u) is toward the Greenland shelf. Unless otherwise stated we use the gridded product of Harden et al. (2016). To create vertical sections, the different variables were gridded using a Laplacian-spline interpolator. The temporal resolution of the grid was

8 hours, the vertical resolution 50 m, and the horizontal resolution 8 km. The distance between the moorings ranged from 8 to 20 km, and with a Rossby radius of deformation in this region of 5 to 10 km (Nurser and Bacon 2014), we likely did not resolve individual eddies that passed through the mooring array.

During the deployment the sea ice cover varied from ice-free conditions in fall to almost full ice cover across the 5 moorings during periods in spring (not shown). The substantial sea ice cover should be kept in mind when interpreting our results.

a. Auxiliary data

1) Sea surface height anomalies from satellite altimetry

The altimeters aboard the Envisat satellite measured sea surface height in Denmark Strait between 2002 and 2012. The delayed-time along-track sea level anomalies, calculated as the difference between the sea surface height and a 20-year mean, were obtained for the entire period. The altimeter products were produced by Ssalto/Duacs and distributed by Aviso, with support from Cnes (AVISO 2016). We use the filtered delayed-time product with a typical resolution of 14 km. Data points affected by sea ice were removed as a part of the data processing. We use only data from the months of August-October when the area around the mooring array was mostly ice free. The data were averaged in 25 km $\times$ 25 km bins.

2) Historical data

To supplement our analysis of the shelfbreak EGC, we include current meter (RCM) data from moorings deployed between KGA 11 and KGA 10 (where the bottom depth is 800 m) in the 1980s and 1990s (Jónsson 1999). The current meters were typically positioned in the deeper part of the water column, but, during three of the years, velocity measurements were obtained closer to the surface as well (at 170 m in 1988-89, and at 80 m in 1990-91 and 1995-96).

3. Mean structure of the shelfbreak EGC

a. Velocity

The mean along-stream velocity field of the shelfbreak EGC revealed a well-defined southwestward-flowing current just offshore of the shelfbreak, centred close to KGA 11 (Fig. 4a). The current was surface-intensified with a core velocity exceeding 20 $\mathrm{cms^{-1}}$ and a width of approximately 30 km. Outside the core of the current the mean flow decreased sharply to just a few $\mathrm{cms^{-1}}$ toward the southwest, both across the deeper part of the Blosseville Basin and on the Greenland shelf.

The standard deviation of the velocity was largest (up to 17 $\mathrm{cms^{-1}}$) in the surface layer close to and offshore of the core of the current (Fig. 4b). As elaborated on below, this was due both to meandering of the current as well as pulsing of the flow. Near the shelfbreak the area of increased variability extended toward the bottom. A second surface-maximum in variability was present close to mooring KGA 8 (discussed in Sect. 4). Across the deeper part of the Blosseville Basin the variability was small, mostly less than 5 $\mathrm{cms^{-1}}$.

b. Hydrography

The surface-intensified shelfbreak EGC was the result of strongly tilted isopycnals close to the shelfbreak, and the core of the current was located above the steepest portion of the sloping interface between the surface layer and the intermediate layer separated by the $\sigma_\theta = 27.7$ $\mathrm{kgm^{-3}}$ isopycnal. Following Harden et al. (2016) we present median fields of hydrographic properties with corresponding inter-quartile ranges to best represent the annual average. The median temperature and salinity fields (Figs. 4c and 4e) revealed a three-layered structure. Near the surface the cold and relatively fresh Polar Surface Water (PSW) covered the entire section, with the coldest and freshest waters toward the Greenland shelf. This layer gradually thinned southeastward from the shelf to around 100 m over the deep part of the Blossville Basin. The warmer and more saline Atlantic-origin Water, bounded by the 0 °C isotherms (indicated by the white contours in Fig. 4c, Våge et al. 2011), occupied the intermediate layer. This water mass had a maximum temperature in the median field of just above 1.1 °C between 300 and 400 m depth. In the same layer the salinity gradually increased with depth toward a maximum around 34.93 at 500-600 m depth (Fig. 4e). In the deep layer the temperature gradually decreased with depth while the salinity remained relatively constant around 34.91-34.92. For a thorough description of the water masses in the EGC, see Rudels et al. (2002, 2005).

Similar to the variability in the velocity field, the interquartile range of temperature and salinity was largest in the surface layer. For temperature, the variability was enhanced throughout the section, whereas the changes in salinity were largest close to the shelfbreak and the core of the current. This was related to lateral shifts of the front between the PSW and the offshore water masses during winter. In periods when the PSW covered the entire section, the salinity, particularly close to the shelfbreak, decreased as fresher water from the shelf was diverted offshore. Due to fairly uniform temperatures within the PSW such lateral shifts only modestly affected the temperature close to the shelfbreak. On the other hand, when the PSW was more constrained to the shelf and upper slope the temperature variability offshore increased as the warmer Atlantic-origin Water reached shallower depths.

4. Variability

The along-stream velocity from September 2011 through July 2012 at 100 m, revealed that the shelfbreak EGC varied in strength and that its core shifted laterally on occasion (Fig. 5), consistent with the standard deviation of the along-stream velocity (Fig. 4b). A striking feature was the strong reversal of the current during November. At that time the current was flowing northward over the shelfbreak and slope, accompanied by a strengthening of the southwestward flow at KGA 8 in the eastern part of the domain. de Steur et al. (2017) used sea level anomaly data from satellite altimeters to show that this was connected with the passage of a large (100 km wide) anti-cyclone. Following this event the opposite situation occurred in January: a strengthening of the southwestward flow over the shelfbreak coincident with a weak reversal at KGA 8. This resembled the passage of a large cyclone, but due to the presence of sea ice during this time of year de Steur et al. (2017) could not use the altimetry data for verification. Such variability across the central basin was evident from the increased standard deviation of the along-stream velocity close to KGA 8 (Fig. 4b).

To analyze the variability of the along-stream velocity of the shelfbreak EGC in more detail, we used empirical orthogonal functions (EOFs). By decomposing the velocity field into orthogonal functions, we extracted the spatial patterns of the dominant variability in the timeseries, their temporal variability, and their contributions to the total variance.

a. Spatial variability

The first EOF mode can be characterized predominantly as a pulsing mode, representing a strengthening and weakening of the shelfbreak EGC (Fig. 6a), i.e. at positive amplitudes the current was stronger than the mean, and at negative amplitudes weaker than the mean. This mode explained 41 % of the variance with the maximum signal between KGA 9 and 10, offshore of the core of the current. The variability was surface-intensified and extended laterally over a broader region than the mean current. This indicated that pulses in the flow were also associated with a widening of the current. The second EOF mode, explaining 17 % of the variance, had a dipole structure which represented lateral shifts of the flow. At times when the flow was weaker than the mean close to the shelfbreak it strengthened offshore and vice versa. This was likely due to a meandering of the shelfbreak current (Fig. 6b), although it could be the signal of eddies altering the velocity structure of the current while propagating past the array. A cyclonic eddy embedded within the shelfbreak current would strengthen the flow close to the core of the current and weaken it offshore. Conversely, an anti-cyclonic eddy propagating within the current would weaken the shelfbreak current and strengthen the flow offshore. The presence of eddies in these cases would mimic a meandering of the current.

In addition to the spatial fields presented in Fig. 6, the EOF calculation returned timeseries of the corresponding principal components (PC) representing the temporal variability of the associated modes. The evolution of the PCs will be discussed more in Sect. 4b, but here we use their standard deviations to illustrate the different velocity fields associated with the dominant modes. By multiplying the standard deviation of the first PC with the first dominant mode and adding this to the mean velocity field, we illustrate the typical flow field for a strong pulse (Fig. 6c). Similarly, the typical flow field for a weak pulse was illustrated by a subtraction of the product of the standard deviation of the first PC and the fist dominant mode from the mean velocity field (Fig. 6e). During a strong pulse (Fig. 6c) the shelfbreak current dominated the section with southwestward flow extending from the shelf to the deep part of the Blosseville Basin. In the opposite phase the shelfbreak current was strongly reduced and confined to the upper slope. Offshore of the current there was a weak flow reversal. We did the same calculation for the second EOF mode. When the shelfbreak EGC meandered onshore the flow was mainly confined to the upper 800 m on the

Greenland slope (Fig. 6d). Conversely, during an offshore meander the current became weaker, wider, and had a deeper extension (Fig. 6f).

We note that the EOF analysis was carried out using the gridded velocity for the entire year. To ensure that the strong reversal of the shelfbreak EGC during November did not dominate the results, the method was also applied to the data excluding this period. This led to qualitatively similar results, with approximately the same explained variances for the two dominant EOF modes. The calculation was not very sensitive to the lateral extent of the domain. The modes of variability from an EOF analysis are technically only modes of the data, which sometimes can be hard to interpret in terms of physical processes. However, the lack of sensitivity to time period and domain size indicates that the modes computed here were robust. Furthermore, the two dominant modes showed well-behaved velocity fields that were physically meaningful. Notably, the patterns of the two modes were readily apparent from inspection of the individual along-stream velocity sections.

b. Temporal variability

Both of the PCs for the two dominant EOF modes displayed seasonality with increasing amplitudes (both positive and negative) over longer periods of time in winter compared to summer (Fig. 7). The reversal of the shelfbreak EGC in autumn was visible as the extended period of negative values in PC1 from late October to the beginning of December. Following this, the amplitudes stayed mostly positive and relatively strong until April, when the strength of the pulsing decreased. There was no such evidence of longer periods of similar sign in PC2, but from approximately April onward the amplitudes were relatively small and the meandering of the current was reduced. PC1 was significantly correlated ($r = 0.69$) with the strength of the current at 100 m. This gives us confidence that pulses in the velocity field were captured by the first mode. From both the Hovmöller diagram (Fig. 5) and the EOF analysis (Figs. 6 and 7) it is evident that the current exhibited both temporal and spatial variability on timescales of days to weeks, in addition to a pronounced seasonal variability.

c. Eddy Kinetic Energy (EKE)

As shown above, the shelfbreak EGC fluctuated both in time and space on various scales. We now compute the eddy kinetic energy (EKE) in the current both from moored observations (the Kögur array (EKE_{moor}) and earlier deployments in the same region (EKE_{hist})) and from satellite measurements (EKE_{alt}). These estimates are used to shed light on the nature of the variability of the shelfbreak EGC.

EKE can be expressed as:

$$EKE = \frac{1}{2}(v'^2 + u'^2) \tag{1}$$

where v' and u' are anomalies relative to the mean of the along-stream and cross-stream velocities, respectively. The procedure to calculate EKE is detailed below for the different types of observations.

1) Estimate of EKE from the Kögur moorings

To analyze the fluctuations in EKE_{moor} on intermediate timescales, we considered the 2-14 day band-pass filtered data. We used 2 days as a lower limit to remove tidal currents and inertial oscillations (which have period around 13 hours), and 14 days as an upper limit to remove longer term variability. The results indicate a surface-intensification of the EKE_{moor}, as revealed by the higher values at 100 m (Fig. 8a) compared to those at 300 m (Fig. 8b). The period from late October through November was noticeably distinct from the other periods, with high values across the northwestern part of the mooring array. This corresponded to the November reversal of the shelfbreak current (Fig. 5). Besides the very strong EKE_{moor} in November, the current was generally more energetic close to the shelfbreak throughout the year, particularly evident in the estimate from 300 m (Fig. 8b). From April onward the variability was strongly reduced. We note that the width of the band-pass filter had some effect on the magnitude of the EKE_{moor}, but not on the pattern shown in Fig. 8.

With only one year of data we cannot robustly quantify the seasonal signal and assess whether 2011-2012 was an anomalous year, or if other years exhibit the same seasonal pattern. Furthermore, we don't know the geographical extent of the elevated EKE_{moor}, and whether these events were confined to the area near the Kögur line or if the entire region was more energetic. We now consider mooring timeseries from previous years along with satellite observations to put the Kögur EKE_{moor} results into a broader geographical and temporal perspective.

2) Estimate of EKE from satellite altimetry data

Sea level anomaly measurements obtained by satellite altimetry allow for the estimation of EKE_{alt}. We used the along-track filtered data from the Envisat satellite to calculate gradients in sea level anomalies (Lilly et al. 2003). Through geostrophy, the along-track sea-surface height anomalies (η') can be converted into cross-track velocity anomalies

$$u' \propto \frac{\partial \eta'}{\partial y} \tag{2}$$

If we further assume isotropy, where u' $\propto$ v', EKE_{alt} can be expressed as

$$EKE_{alt} = \frac{1}{2}(u'^2 + v'^2) = u'^2 \tag{3}$$

Using the moored measurements we examined the assumption of isotropy and found that it was generally justified. The use of satellite altimetry data is limited by the presence of sea ice, which covered the mooring array during large parts of the year. From climatological values of sea ice concentration (not shown) we know that the east Greenland shelf is typically covered by sea ice from late November through May. Hence, we present results from August to October for the estimate of EKE_{alt} for comparison with our mooring-based estimate EKE_{moor}. Due to the strongly skewed distribution of individual estimates we used the median as a measure of the typical EKE_{alt} in this region.

At this time of year, the highest EKE_{alt} throughout the Nordic Seas was found near Denmark Strait (not shown). A similar method for estimating EKE_{alt} from satellite altimetry was used by von Appen et al. (2016) across the West Spitsbergen Current in the northeastern part of the Nordic Seas. They found that August was the calmest period of the year, with EKE_{alt} values in winter of comparable magnitude to our August to October values. Bulczak et al. (2015) used sea surface height measurements from the Envisat satellite similar to our estimates to compare EKE_{alt} from summer and winter across the entire Nordic Seas. Their analysis showed that the east Greenland shelfbreak region was more energetic in winter than in summer, and they attributed this to an interplay between sea ice, bathymetry, wind, and oceanic processes. Focusing on the Denmark Strait (Fig. 9), two regions of enhanced EKE_{alt} were revealed: along the shelfbreak south of 70°N and just downstream of the sill. The latter maximum likely results from generation of cyclones or intensification of existing cyclones south of Denmark Strait as the overflow plume descends the continental slope (Bruce 1995; Spall and Price 1998; von Appen et al. 2014). The average EKE_{alt} for the 9 years of satellite data in the vicinity of the mooring array was similar to the values estimated from the Kögur observations during October 2011 (even though the mooring-based estimate was calculated from the timeseries at 100 m and the satellite measurements represent surface conditions). The model results of Våge et al. (2013) suggest that the bend in the bathymetry near 70°N at the northern end of the Blosseville Basin is a critical point in the formation of eddies from the shelfbreak EGC through baroclinic instability. In this region the wind typically does not have a substantial component that is parallel to the shelfbreak, and hence the Ekman transport does not suppress instabilities through frontogenesis. This suggests that the enhanced EKE_{alt} near the shelfbreak in Fig. 8 was due in part to eddies propagating past the array.

3) Estimate of EKE from historical data

We now compare estimates of EKE_{hist} from three previous years (1988-89, 1990-91, and 1995-96) with the year 2011-2012. The aim is to assess the apparent seasonal variability, and also to elucidate whether the highly energetic period associated with the November reversal of the current was anomalous. Recall that the earlier moorings were deployed between KGA10 and KGA11 (see the Data and Methods section).

The comparison of the timeseries of EKE_{hist} for the 4 years shows that the current typically was more energetic during late fall and early winter, and less so during summer (Fig. 10). The two timeseries which covered the entire summer showed very weak variability in July and August. The high EKE_{moor} in November 2011 associated with the reversal of the shelfbreak EGC did not seem to be unique and occurred to some extent in every deployment (Fig. 10). In particular, the timeseries from 1990-91 showed similarly high EKE_{hist}, both during December and March. In common for these high eddy energy events was a decrease in the strength of the background current (not shown). We speculate that this could be due to eddy formation or instabilities in the shelfbreak EGC, near the mooring location or farther upstream, which would tend to weaken the background flow at the mooring location. For the highest EKE_{hist} values, the current strength was not only reduced but at times the current even reversed, similar to the November 2011 reversal (not shown). We discuss this extraction of energy from the mean flow by eddy formation further in the next section.

5. Stability of the current

The high levels of EKE_{moor} associated with the shelfbreak EGC in the mooring records (Fig. 8), combined with the enhanced surface EKE_{alt} along the shelfbreak south of 70°N (Fig. 9), motivate us to address the stability characteristics of the current using the Kögur timeseries.

a. Barotropic instability

The barotropic energy conversion (BT) is a measure of the kinetic energy extracted from the mean flow by eddies. The momentum extracted is transported down the mean lateral velocity gradient (Spall et al. 2008). Barotropic conversion is estimated as

$$BT = -\rho_0 \overline{v'u'} \frac{\partial \overline{v}}{\partial x}, \tag{4}$$

where ρ_0 is a reference density of 1027 kgm^{-3}, $\overline{v'u'}$ is the average eddy momentum flux calculated from the 2-14 day band-passed data, and $\frac{\partial \overline{v}}{\partial x}$ is the average lateral velocity gradient. We use a low-pass filter with a cutoff frequency of 14 days as an averaging operator for both of these quantities. A high positive BT indicates that kinetic energy in the mean flow is converted into eddy energy. Generally, a strong horizontal velocity gradient is beneficial for the development of barotropic instability, whereas a steep bathymetric slope tends to suppress it. The Kögur observations indicate that the BT strongly increased close to the shelfbreak during the November reversal (Fig. 11a). This was mostly due to strong horizontal velocity gradients when the current reversed. Starting in December BT abruptly declined and remained low for the rest of the deployment period. We note that the barotropic conversion generally changed sign near the shelfbreak. This was due to the reversed horizontal velocity gradient on either side of the core of the current.

To investigate whether the high BT in late fall and early winter was the result of barotropic instability of the shelfbreak EGC, we considered the necessary condition for such instabilities to form, which is that the lateral gradient in potential vorticity within the current changes sign. This is related to a change in sign of $\beta - \partial^2 v/\partial x^2$ (Cushman-Roisin and Beckers 2011). The topographic β in this region is quite large with typical values of O(10^{-6} – 10^{-7} s^{-1}m^{-1}) due to the steep slope, hence a strong horizontal gradient in along-stream velocity is required to overcome the stabilizing effect of topographic β. Typical velocities in the shelfbreak EGC were around 0.5 ms^{-1}, but at times the current reached 1 ms^{-1}. The width of the current varied but was typically 20 to 30 km. This gave a $\partial^2 v/\partial x^2$ of O(10^{-9} s^{-1}m^{-1}). A reduction of the current width to 5 km would still not be sufficient to increase $\partial^2 v/\partial x^2$ above the topographic β, and hence the necessary condition for barotropic instability appeared not to be fulfilled, at least not at the location of the mooring array. The barotropic conversion, however, showed a very strong signal during the November reversal, indicating that barotropic instabilities could have taken place at this time. However, since the necessary condition was not fulfilled, these instabilities would have had to be triggered upstream and propagate to the mooring location with the mean flow. For the remainder of the year the barotropic conversion was relatively low, consistent with the condition for barotropic instability not being satisfied.

b. Baroclinic instability

The baroclinic energy conversion (BC) represents the available potential energy extracted from the mean flow by eddies. The potential energy extracted is transported down the mean lateral density gradient (Spall et al. 2008). The baroclinic conversion is estimated as

$$BC = -g\frac{\partial z}{\partial x}\overline{u'\rho'} = g\left(\frac{\partial\overline{\rho}}{\partial x}/\frac{\partial\overline{\rho}}{\partial z}\right)\overline{u'\rho'}, \tag{5}$$

where g is the gravitational acceleration, $\frac{\partial z}{\partial x}$ is the average slope of the isopycnals, and $\overline{u'\rho'}$ is the average eddy density flux calculated from the 2-14 day band-passed data. We use a low-pass filter with a cutoff frequency of 14 days as an averaging operator for both of these quantities. The horizontal density gradient is related to the vertical velocity shear through the thermal wind equation such that $\frac{\partial v}{\partial z} \propto \frac{\partial \rho}{\partial x}$. This relationship is valid for flow in geostrophic balance, which is largely the case for the shelfbreak EGC (not shown). A strong vertical velocity shear favors baroclinic instability, while a strong vertical density gradient (i.e. strong stratification) suppresses it. Due to a large eddy density flux combined with a large horizontal density gradient, the shelfbreak EGC showed a particularly high baroclinic conversion during October, November, and into mid-December (Fig. 11b). Several episodes of high BC took place throughout the winter, in particular close to the core of the current. From approximately April onward the conversion and its variability was greatly reduced. This corresponds well to the reduced current variability discussed above in terms of the PCs and the estimates of EKE_{moor} and EKE_{hist}.

A necessary, but not sufficient, condition for baroclinic instability is that the horizontal gradient of potential vorticity changes sign with depth. The potential vorticity is the sum of several terms (see e.g. Spall et al. (2008) and von Appen and Pickart (2012) for a description of each term). However, the planetary potential vorticity was by far the dominant term, which can be calculated as

$$PV = \frac{f}{\rho}\frac{\partial \rho}{\partial z}, \tag{6}$$

where f is the Coriolis frequency and ρ is the potential density. The mean PV field (not shown) indicated that the condition for baroclinic instability was fulfilled. In particular, the horizontal PV gradient was positive in the upper layer near the core of the current and negative below this.

It is of interest to contrast periods when the shelfbreak EGC was highly varying (high EKE_{moor}) versus periods when the current was more stable (low EKE_{moor}). We omit the period of the November reversal from this analysis as this would completely dominate the results. Instead we focus on the current variability during its “normal” state, i.e. when it was directed toward the southwest. To select periods of unstable and stable conditions we consider times when the EKE_{moor} was greater than its 90th percentile value and lower than its 10th percentile value, respectively. We chose these limits in order to have a reasonable sample size; small changes to the threshold values did not qualitatively affect the results.

Consistent with our previous findings, the unstable periods took place during fall and winter, while most of the stable periods occurred in late spring and summer (Fig. 12). To assess the differences between the two states we made composites of the along-stream velocity and density. In the unstable case the shelfbreak EGC had two maxima (Fig. 13a). This was similar to the configuration of the current when it meandered offshore, as shown by the second EOF (Fig. 6f). In the case of a stable, weakly energetic shelfbreak current the along-stream velocity field resembled the mean state with a surface-intensified current close to the shelfbreak (Fig. 13b). The contrast between the states becomes clearer when we consider the difference between the two (Fig. 13c). Baroclinic instability typically leads to the formation of dipole eddy pairs where the anti-cyclone is associated with the meandering of the current and the cyclone forms farther offshore, adjacent to the meander (e.g. Spall 1995). This is similar to the composite mean of the unstable state where an anti-cyclonic pattern was evident (Fig. 13c). An interpretation of this result may be that during times when the current meanders and the meanders grow, we observe a highly variable current where energy is transferred from the mean flow to the eddy field.

6. Summary and discussion

The analysis of a year-long mooring data set from the shelfbreak EGC north of Denmark Strait has revealed a highly dynamic current with a varying spatial structure. The two dominant modes of variability are a pulsing mode and a meandering mode, both of which had an apparent seasonal signal. Their corresponding principal component timeseries showed strong variability during fall and winter, whereas during summer the current was more quiescent and mostly located close to the shelfbreak. While a single year of data is not enough to robustly determine the seasonal variability, the observed changes in the Kögur data are consistent with previous moored measurements from the shelfbreak EGC. In particular, Jónsson (1999) documented seasonal variability of the shelfbreak EGC based on monthly mean velocities at depth from four years during the period 1988 to 1996 (the same mooring used in Fig. 10).

At the Denmark Strait sill, long-term observations within the DSOW plume reveal that seasonality can explain only around 5 % of the variability in the transport timeseries (Jochumsen et al. 2012). Farther upstream, this lack of seasonal variability was supported by the results of Harden et al. (2016), who found a steady supply of DSOW through the Kögur section throughout the year. Note, however, that both of these results represent the aggregate transport of DSOW from all branches flowing toward Denmark Strait. Hence, while the shelfbreak EGC appears to vary seasonally, this has only limited impact on the total transport of DSOW into the North Atlantic. The shelfbreak EGC may, however, strongly influence the short-term variability observed at the Denmark Strait sill.

Using the same measurements employed in this study, de Steur et al. (2017) estimated the freshwater transport (FWT) through the Kögur section. They found that the FWT was strongly affected by the variability in the shelfbreak EGC, and that at the time of the November flow reversal the section-wide FWT toward Denmark Strait was close to zero. Our results show that most of the current variability takes place in the upper water column, and hence the variability was more important for the flux of light surface waters compared to the transport of DSOW. In fact, due to the large amount of freshwater in the upper water column across the east Greenland shelf and slope, the variability of the shelfbreak EGC largely governs the FWT north of Denmark Strait (de Steur et al. 2017).

Previous characterizations of the kinematic structure of the shelfbreak EGC north of Denmark Strait were largely based on shipboard sections of hydrography and velocity occupied in summer, depicting it as a southwestward-flowing current situated near the shelfbreak (Nilsson et al. 2008; Våge et al. 2013; Håvik et al. 2017). However, the strong reversal of the shelfbreak EGC during November, discussed by Harden et al. (2016) and de Steur et al. (2017), has changed our perception of this current branch. de Steur et al. (2017) described this event as a large anti-cyclone passing by the mooring array over a period of more than a month. We have shown here that, coincident with the large-scale changes in the current, it also exhibited substantial variability on shorter timescales. In fact, during the event the variability on periods of 2-14 days were by far the highest throughout the year (Fig. 8). At this time there was also enhanced barotropic and baroclinic mean-to-eddy energy conversion. The frequency of such flow reversals is not known, but our estimate of EKE_{hist} from four years of velocity measurements (Fig. 10) indicate that, to some degree, these highly energetic events are not uncommon.

While this study has focused on internal oceanic processes that lead to variability in the shelfbreak EGC, wind forcing and the presence of sea ice undoubtedly contribute to the observed variability. Previous work has shown that wind is important for the separation of the EGC at the northern end of the Blosseville Basin (Våge et al. 2013). In addition, Harden et al. (2016) argue that the partitioning of transport between the NIJ and the EGC system is predominantly governed by regional changes in the wind stress curl. Although it was not addressed in this study, the seasonal pack ice likely modulates the behavior of the shelfbreak EGC. For example, past studies have demonstrated that freely moving ice keels allow for a more effective transfer of wind stress from the atmosphere to the ocean (e.g. Schulze and Pickart 2012). This warrants further consideration using the Kögur data.

The highest surface EKE_{alt} values in the Nordic Seas, for the period August to October, occur in the Denmark Strait region. We believe that this is largely due to the shelfbreak EGC meandering and/or forming eddies north of the sill. We demonstrated that the current was conducive for baroclinic instability during fall, winter, and early spring. However, barotropic instability could also play a role during periods of strong horizontal velocity gradients, although our data are not conclusive in this regard. We further suggest that eddies formed by baroclinic instability in the shelfbreak EGC may be one of the sources of the variability observed at the Denmark Strait sill, and that the substantial short-term variability previously documented at the sill (Mastropole et al. 2017; von Appen et al. 2017) and across the Kögur section (Harden et al. 2016) is reflected by the high values of EKE.

Acknowledgments. Support for this work was provided by the Norwegian Research Council under Grant agreement 231647 (LH and KV), and the Bergen Research Foundation (KV). Additional funding was provided by the National Science Foundation under grants OCE-0959381 and OCE-1558742 (RP).

References

AVISO, 2016: AVISO Satellite Altimetry Data: SSALTO/DUACS multimission altimeter products. Accessed September 2016. Available online at http://www.aviso. altimetry.fr/duacs/.

Bruce, J. G., 1995: Eddies southwest of the Denmark Strait. *Deep Sea Research Part I: Oceanographic Research Papers*, **42 (1)**, 13 – 29, doi:10.1016/0967-0637(94)00040-Y.

Bulczak, A. I., S. Bacon, A. C. Naveira Garabato, A. Ridout, M. J. P. Sonnewald, and S. W. Laxon, 2015: Seasonal variability of sea surface height in the coastal waters and deep basins of the Nordic Seas. *Geophysical Research Letters*, **42 (1)**, 113–120, doi:10.1002/2014GL061796.

Cushman-Roisin, B., and J.-M. Beckers, 2011: *Introduction to Geophysical Fluid Dynamics: physical and numerical aspects*, Vol. 101. Academic Press, 768 pp.

de Steur, L., R. S. Pickart, A. Macrander, K. Våge, B. Harden, S. Jónsson, S. Østerhus, and H. Valdimarsson, 2017: Liquid freshwater transport estimates from the East Greenland Current based on continuous measurements north of Denmark Strait. *Journal of Geophysical Research: Oceans*, doi:10.1002/2016JC012106.

Dickson, B., and Coauthors, 2008: *The Overflow Flux West of Iceland: Variability, Origins and Forcing*, 443–474. Springer Netherlands, Dordrecht, doi:10.1007/978-1-4020-6774-7_20.

Dickson, R., B. Rudels, S. Dye, M. Karcher, J. Meincke, and I. Yashayaev, 2007: Current estimates of freshwater flux through Arctic and subarctic seas. *Progress in Oceanography*, **73 (3)**, 210–230, doi:10.1016/j.pocean.2006.12.003.

Harden, B. E., and Coauthors, 2016: Upstream Sources of the Denmark Strait Overflow: Observations from a High-Resolution Mooring Array. *Deep Sea Research Part I: Oceanographic Research Papers*, **112**, 94–112, doi:10.1016/j.dsr.2016.02.007.

Håvik, L., R. S. Pickart, K. Våge, D. Torres, A. M. Thurnherr, A. Beszczynska-Möller, W. Walczowski, and W.-J. von Appen, 2017: Evolution of the East Greenland Current from Fram Strait to Denmark Strait: Synoptic measurements from summer 2012. *Journal of Geophysical Research: Oceans*, doi:10.1002/2016JC012228.

Hogg, N., G. Siedler, and W. Zenk, 1999: Circulation and Variability at the Southern Boundary of the Brazil Basin. *Journal of Physical Oceanography*, **29 (2)**, 145–157, doi:10.1175/1520-0485(1999)029⟨0145:CAVATS⟩2.0.CO;2.

Jeansson, E., S. Jutterström, B. Rudels, L. G. Anderson, K. A. Olsson, E. P. Jones, W. M. Smethie, and J. H. Swift, 2008: Sources to the East Greenland Current and its contribution to the Denmark Strait Overflow. *Progress in Oceanography*, **78 (1)**, 12–28, doi:10.1016/j.pocean.2007.08.031.

Jochumsen, K., D. Quadfasel, H. Valdimarsson, and S. Jónsson, 2012: Variability of the Denmark Strait overflow: Moored time series from 1996-2011. *Journal of Geophysical Research: Oceans*, **117 (C12)**, doi:10.1029/2012JC008244.

Jónsson, S., 1999: The circulation in the northern part of the Denmark Strait and its variability. *ICES Report-CM*, **L:06**, 9pp.

Jónsson, S., and H. Valdimarsson, 2004: A new path for the Denmark Strait overflow water from the Iceland Sea to Denmark Strait. *Geophysical Research Letters*, **31 (3)**, doi:10.1029/2003GL019214.

Lilly, J. M., 2016: jLab: A data analysis package for Matlab, v. 1.6.2. [Available online at http://www.jmlilly.net/jmlsoft.html].

Lilly, J. M., P. B. Rhines, F. Schott, K. Lavender, J. Lazier, U. Send, and E. D'Asaro, 2003: Observations of the Labrador Sea eddy field . *Progress in Oceanography*, **59 (1)**, 75 – 176, doi:10.1016/j.pocean.2003.08.013.

Mastropole, D., R. S. Pickart, H. Valdimarsson, K. Våge, K. Jochumsen, and J. Girton, 2017: On the hydrography of Denmark Strait. *Journal of Geophysical Research: Oceans*, **122 (1)**, 306–321, doi:10.1002/2016JC012007.

Nilsson, J., G. Björk, B. Rudels, P. Winsor, and D. Torres, 2008: Liquid freshwater transport and Polar Surface Water characteristics in the East Greenland Current during the AO-02 Oden expedition. *Progress in Oceanography*, **78 (1)**, 45 – 57, doi:10.1016/j.pocean.2007.06.002.

Nurser, A. J. G., and S. Bacon, 2014: The Rossby radius in the Arctic Ocean. *Ocean Science*, **10 (6)**, 967–975, doi:10.5194/os-10-967-2014.

Rudels, B., G. Björk, J. Nilsson, P. Winsor, I. Lake, and C. Nohr, 2005: The interaction between waters from the Arctic Ocean and the Nordic Seas north of Fram Strait and along the East Greenland Current: results from the Arctic Ocean-02 Oden expedition. *Journal of Marine Systems*, **55 (1)**, 1–30, doi:10.1016/j.jmarsys.2004.06.008.

Rudels, B., E. Fahrbach, J. Meincke, G. Budèus, and P. Eriksson, 2002: The East Greenland Current and its contribution to the Denmark Strait overflow. *ICES Journal of Marine Science: Journal du Conseil*, **59 (6)**, 1133–1154, doi:10.1006/jmsc.2002.1284.

Schulze, L. M., and R. S. Pickart, 2012: Seasonal variation of upwelling in the Alaskan Beaufort Sea: Impact of sea ice cover. *Journal of Geophysical Research: Oceans*, **117 (C6)**, doi:10.1029/2012JC007985.

Smith, P. C., 1976: Baroclinic Instability in the Denmark Strait Overflow. *Journal of Physical Oceanography*, **6 (3)**, 355–371, doi:10.1175/1520-0485(1976)006⟨0355:BIITDS⟩2.0.CO;2.

Spall, M. A., 1995: Frontogenesis, subduction, and cross-front exchange at upper ocean fronts. *Journal of Geophysical Research: Oceans*, **100 (C2)**, 2543–2557, doi:10.1029/94JC02860.

Spall, M. A., R. S. Pickart, P. S. Fratantoni, and A. J. Plueddemann, 2008: Western Arctic Shelfbreak Eddies: Formation and Transport. *Journal of Physical Oceanography*, **38 (8)**, 1644–1668, doi:10.1175/2007JPO3829.1.

Spall, M. A., and J. F. Price, 1998: Mesoscale Variability in Denmark Strait: The PV Outflow Hypothesis. *Journal of Physical Oceanography*, **28 (8)**, 1598–1623, doi:10.1175/1520-0485(1998)028⟨1598:MVIDST⟩2.0.CO;2.

Strass, V. H., E. Fahrbach, U. Schauer, and L. Sellmann, 1993: Formation of Denmark Strait overflow water by mixing in the East Greenland Current. *Journal of Geophysical Research: Oceans (1978–2012)*, **98 (C4)**, 6907–6919, doi:10.1029/92JC02732.

Våge, K., R. S. Pickart, M. A. Spall, G. Moore, H. Valdimarsson, D. J. Torres, S. Y. Erofeeva, and J. E. Ø. Nilsen, 2013: Revised circulation scheme north of the Denmark Strait. *Deep Sea Research Part I: Oceanographic Research Papers*, **79**, 20 – 39, doi:10.1016/j.dsr.2013.05.007.

Våge, K., R. S. Pickart, M. A. Spall, H. Valdimarsson, S. Jónsson, D. J. Torres, S. Østerhus, and T. Eldevik, 2011: Significant role of the North Icelandic Jet in the formation of Denmark Strait overflow water. *Nature Geoscience*, **4 (10)**, 723–727, doi:10.1038/NGEO1234.

von Appen, W.-J., D. Mastropole, R. S. Pickart, H. Valdimarsson, S. Jónsson, and J. B. Girton, 2017: On the Nature of the Mesoscale Variability in Denmark Strait. *Journal of Physical Oceanography*, **47 (3)**, 567–582, doi:10.1175/JPO-D-16-0127.1.

von Appen, W.-J., and R. S. Pickart, 2012: Two Configurations of the Western Arctic Shelfbreak Current in Summer. *Journal of Physical Oceanography*, **42 (3)**, 329–351, doi:10.1175/JPO-D-11-026.1.

von Appen, W.-J., R. S. Pickart, K. H. Brink, and T. W. Haine, 2014: Water column structure and statistics of Denmark Strait Overflow Water cyclones. *Deep Sea Research Part I: Oceanographic Research Papers*, **84**, 110 – 126, doi:10.1016/j.dsr.2013.10.007.

von Appen, W.-J., U. Schauer, T. Hattermann, and A. Beszczynska-Möller, 2016: Seasonal Cycle of Mesoscale Instability of the West Spitsbergen Current. *Journal of Physical Oceanography*, **46 (4)**, 1231–1254, doi:10.1175/JPO-D-15-0184.1.

Woodgate, R. A., E. Fahrbach, and G. Rohardt, 1999: Structure and transports of the East Greenland Current at 75°N from moored current meters. *Journal of Geophysical Research: Oceans*, **104 (C8)**, 18 059–18 072, doi:10.1029/1999JC900146.

LIST OF FIGURES

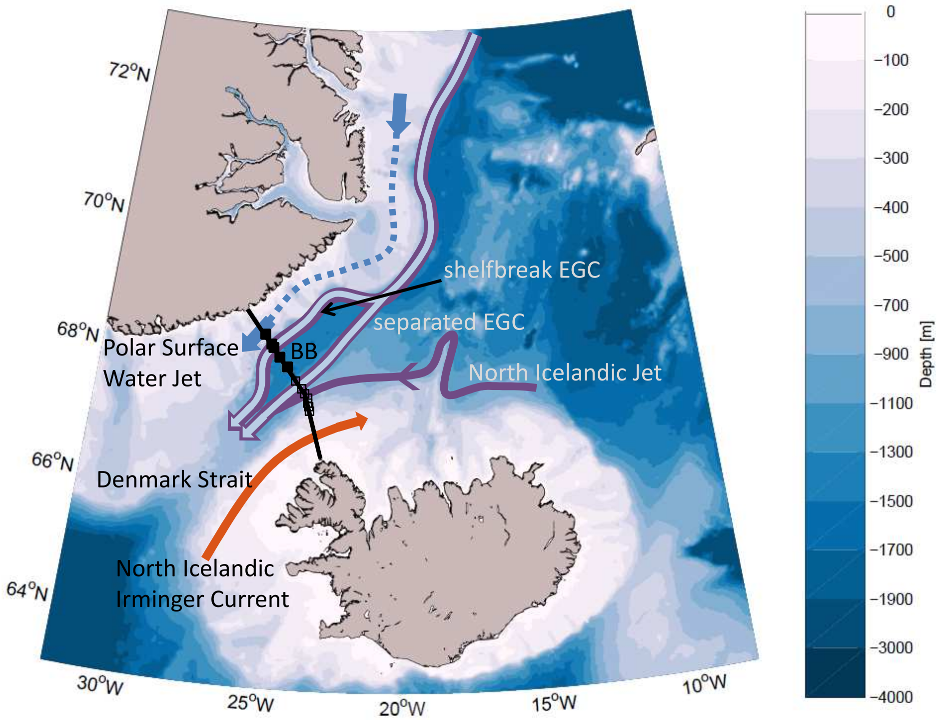

FIG. 1. Schematic overview of the currents in the vicinity of Denmark Strait. The shelfbreak East Greenland Current (EGC) and the separated EGC transport both dense intermediate waters (purple lines) and light surface waters (light blue lines). The North Icelandic Jet transports mostly dense intermediate waters from the Iceland Sea. The dashed line on the shelf represents the Polar Surface Water Jet which transports relatively fresh surface waters. The North Icelandic Irminger Current transports warm and saline Atlantic Water northward into the Iceland Sea along the coast of Iceland. The acronym BB represents the Blosseville Basin. The black line indicates the Kögur transect and the location of the moorings are marked by black squares. Filled squares mark the moorings utilized in this study.

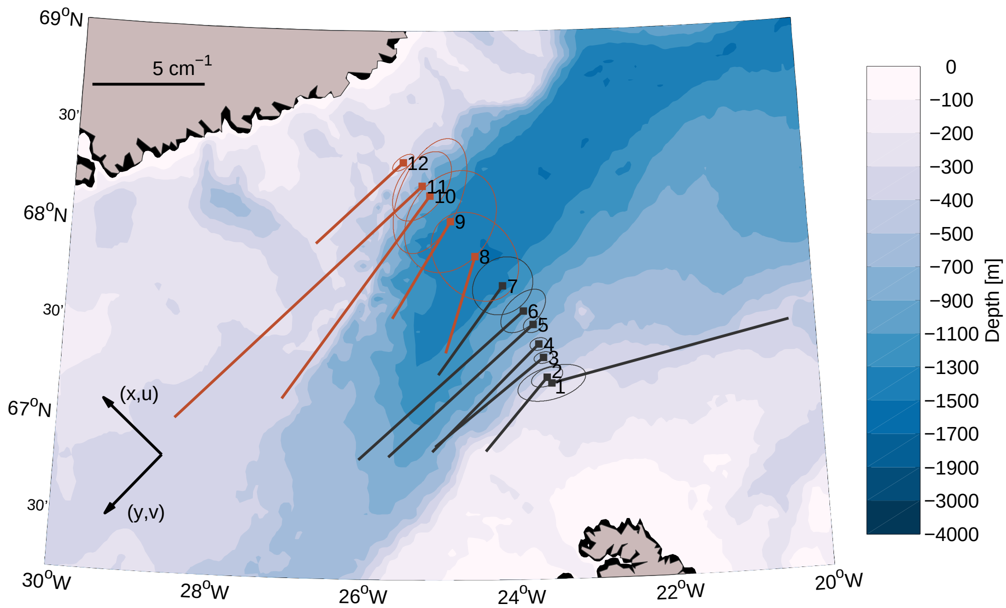

FIG. 2. Depth-integrated current vectors over the upper 500 m with corresponding standard error ellipses. The coordinate system used in the study is rotated 139° counter-clockwise from east, as indicated by the arrows in the lower left corner. The line in the top left corner represents a velocity of 5 cms^{-1}. The moorings used in this study are highlighted in orange.

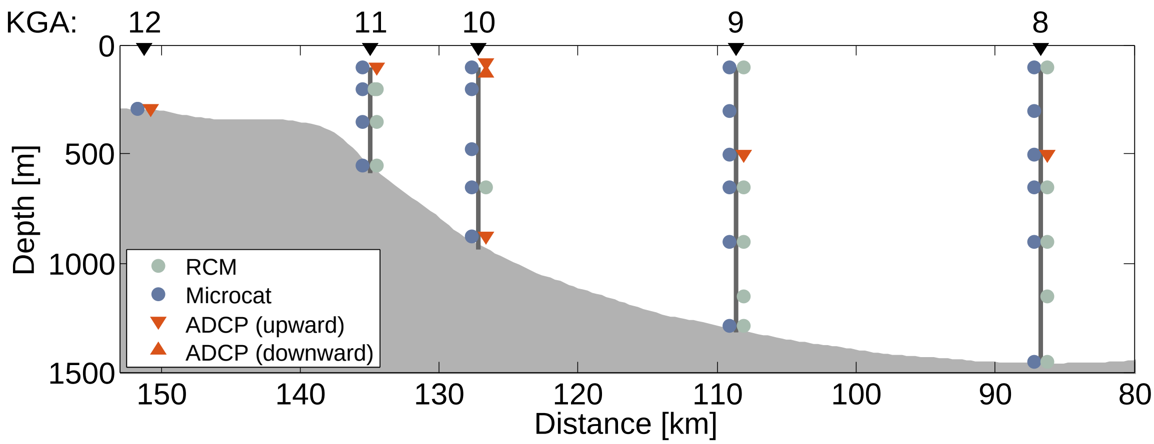

FIG. 3. Bathymetry and instrumentation along the northwestern part of the Kögur transect. The numbers on the top indicate the mooring number and the instrumentation on each mooring is marked by the symbols.

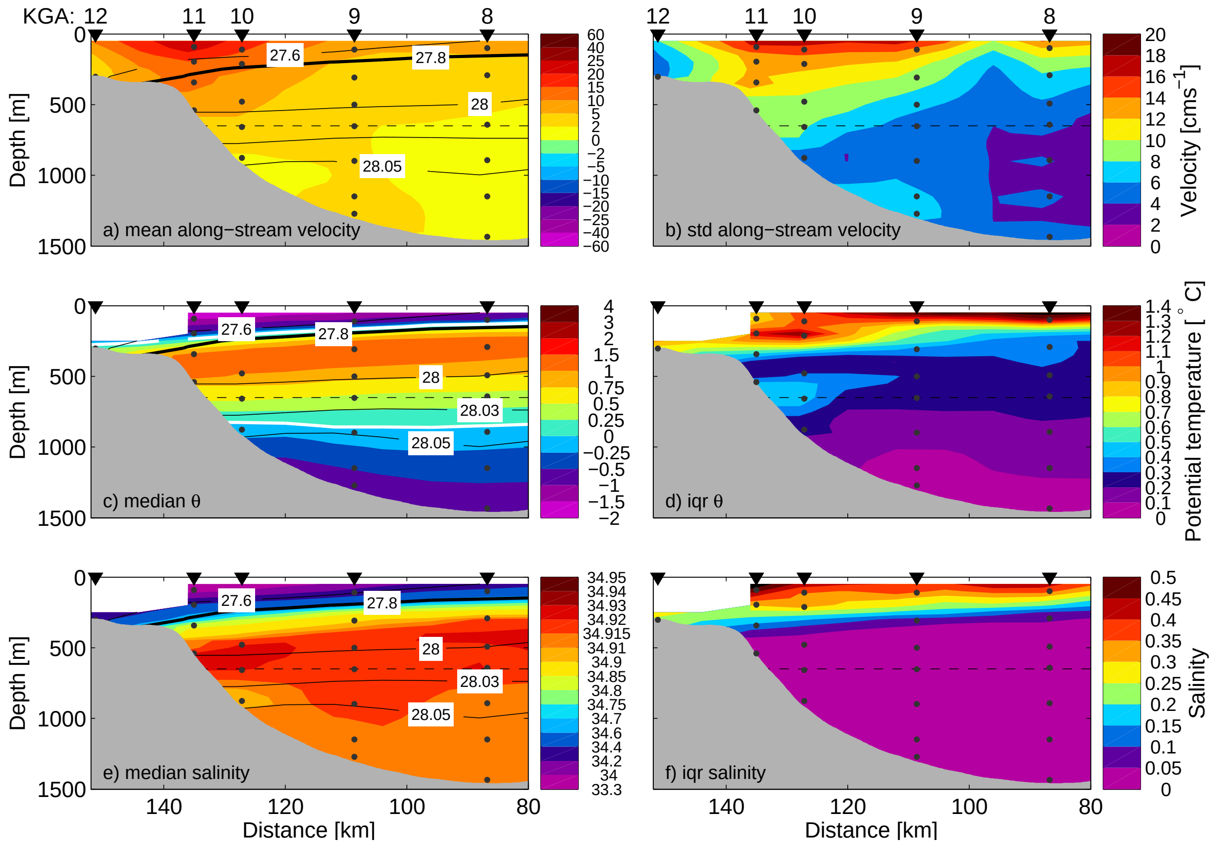

FIG. 4. Vertical sections of year-long mean or median properties (left hand column) and the corresponding standard deviation or interquartile ranges (right hand column). Top row: along-stream velocity; middle row: potential temperature; bottom row: salinity. Positive current speeds are toward the southwest. The mooring locations are indicated on top of each section, and the instruments on each mooring by the black dots. The black contours are median isopycnals, with the 27.8 kgm^{-3} isopycnal (the upper limit for DSOW) highlighted in bold. The dashed line indicates the sill depth of Denmark Strait (650 m). The white contours in c) are the 0 °C isotherms delimiting the Atlantic-origin Water.

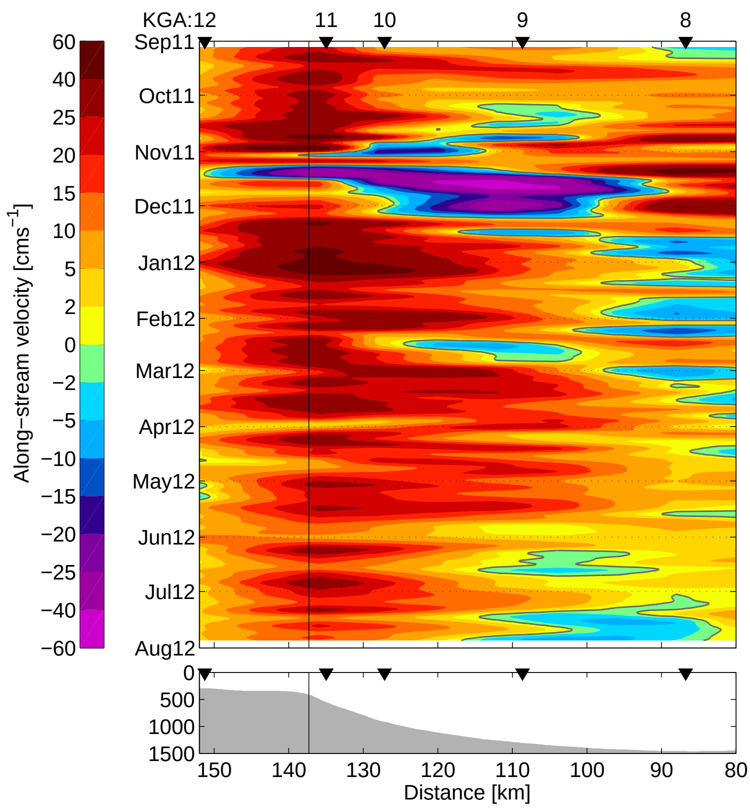

FIG. 5. Hovmöller diagram of 7-day low-pass filtered along-stream velocity of the shelfbreak EGC at 100 m. Positive current speeds are toward the southwest. The gray line is the zero velocity contour. The black vertical line marks the shelfbreak. The bathymetry and the mooring locations are plotted in the lower panel.

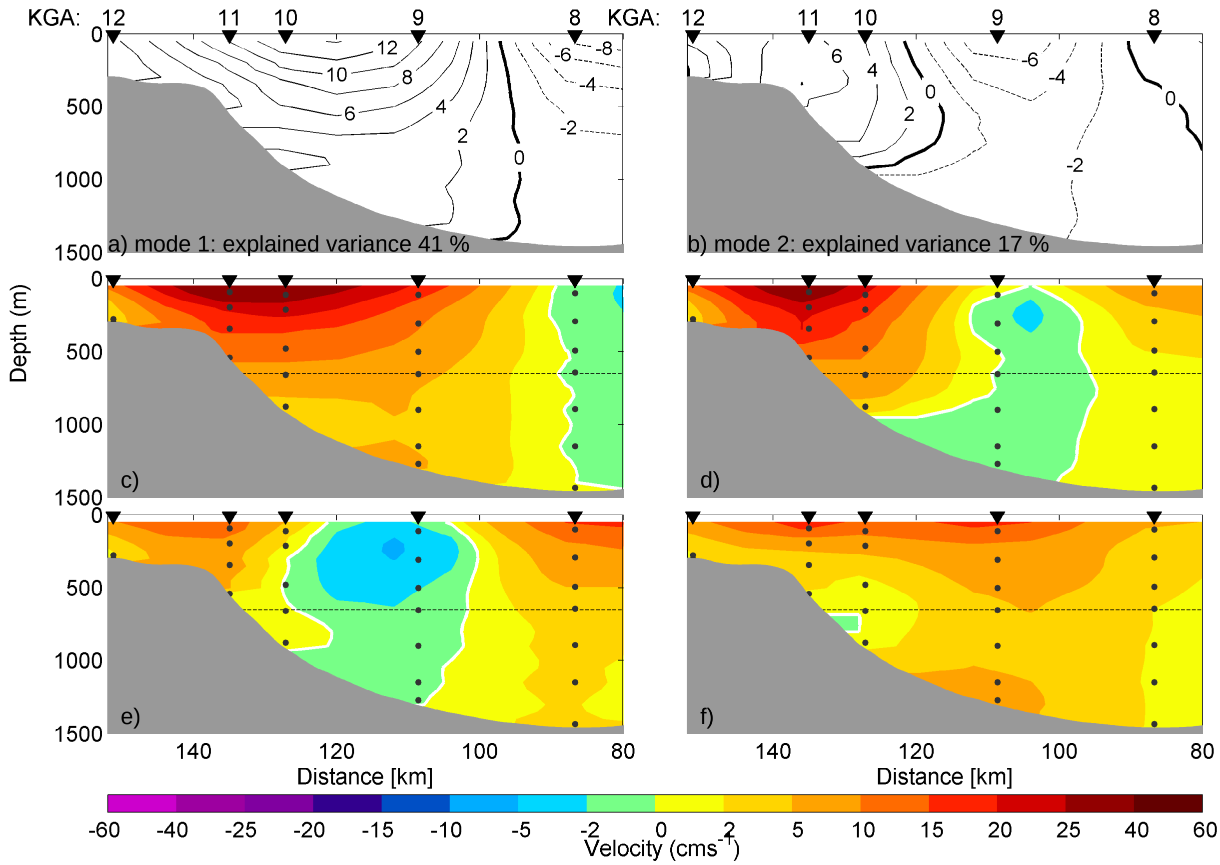

FIG. 6. Empirical orthogonal functions of the along-stream velocity field [cms^{-1}]. The left-hand column is mode 1 (pulsing mode) and the right-hand column is mode 2 (meandering mode). Top row: modal structure; middle row: mean velocity field plus one standard deviation of the modal amplitude; bottom row: mean velocity field minus one standard deviation of the modal amplitude. The mooring locations are indicated on top of each section, and the instruments on each mooring by the black dots. The dashed line indicates the sill depth of Denmark Strait (650 m).

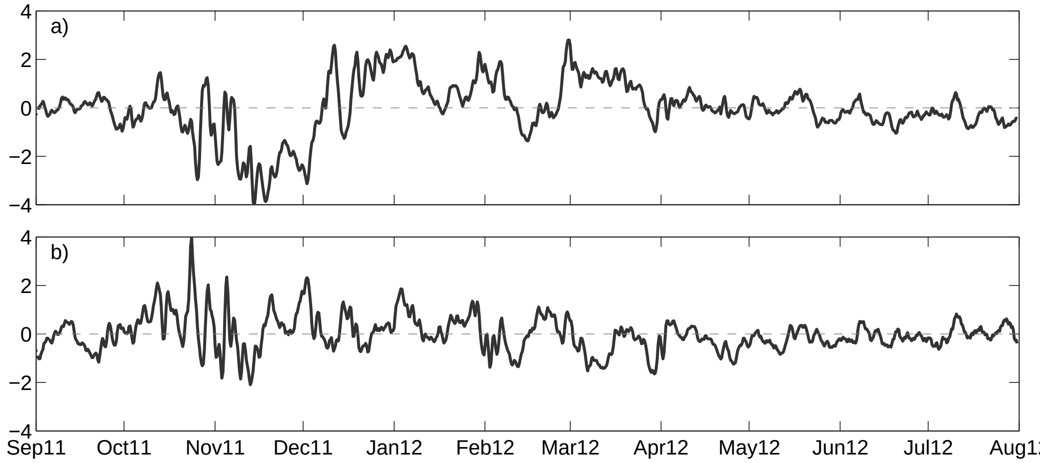

FIG. 7. Principal component timeseries of the first (a) and second (b) EOF modes.

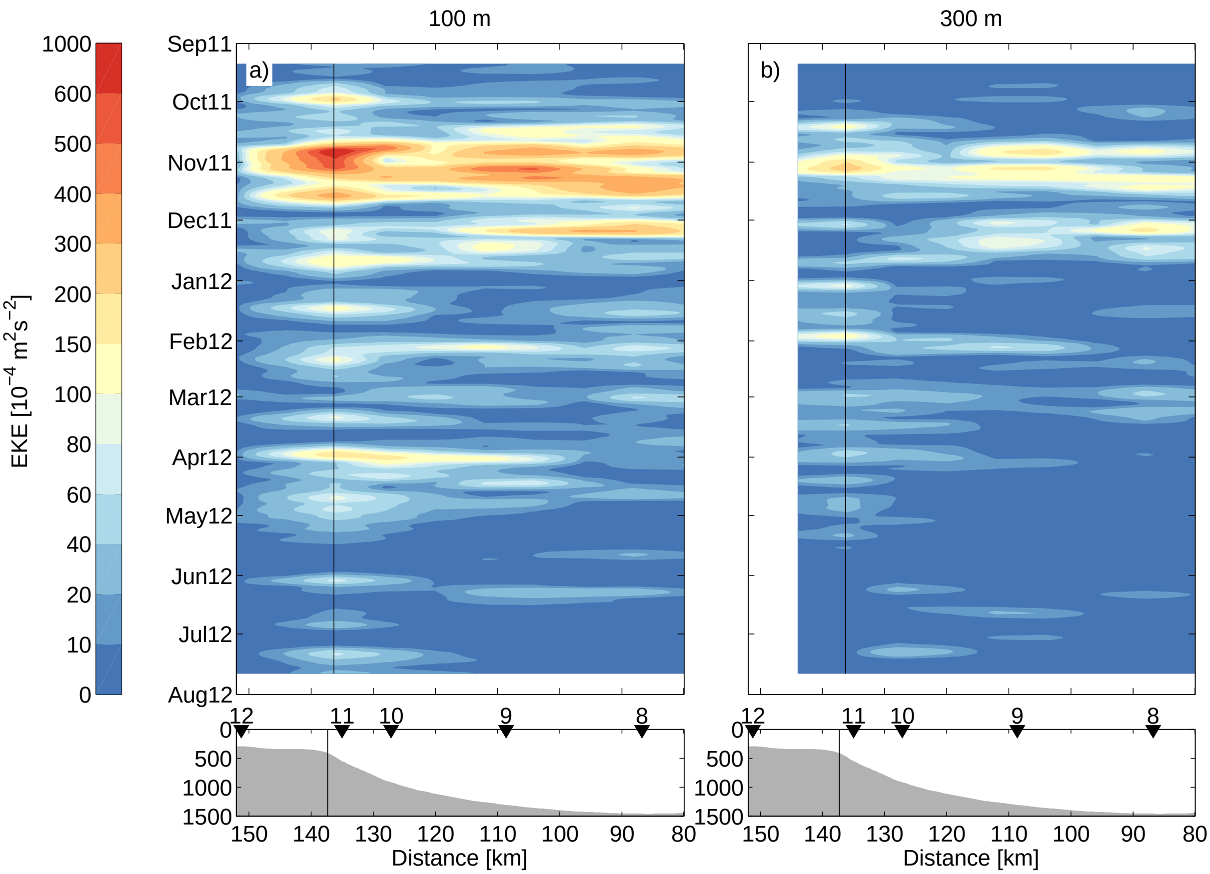

716 FIG. 8. Hovmöller diagrams of the band-pass filtered EKE_{moor} at (a) 100 m and (b) 300 m (see text for details).
717 The black vertical lines indicate the location of the shelfbreak. The bathymetry and the mooring locations are
718 plotted in the lower panels.

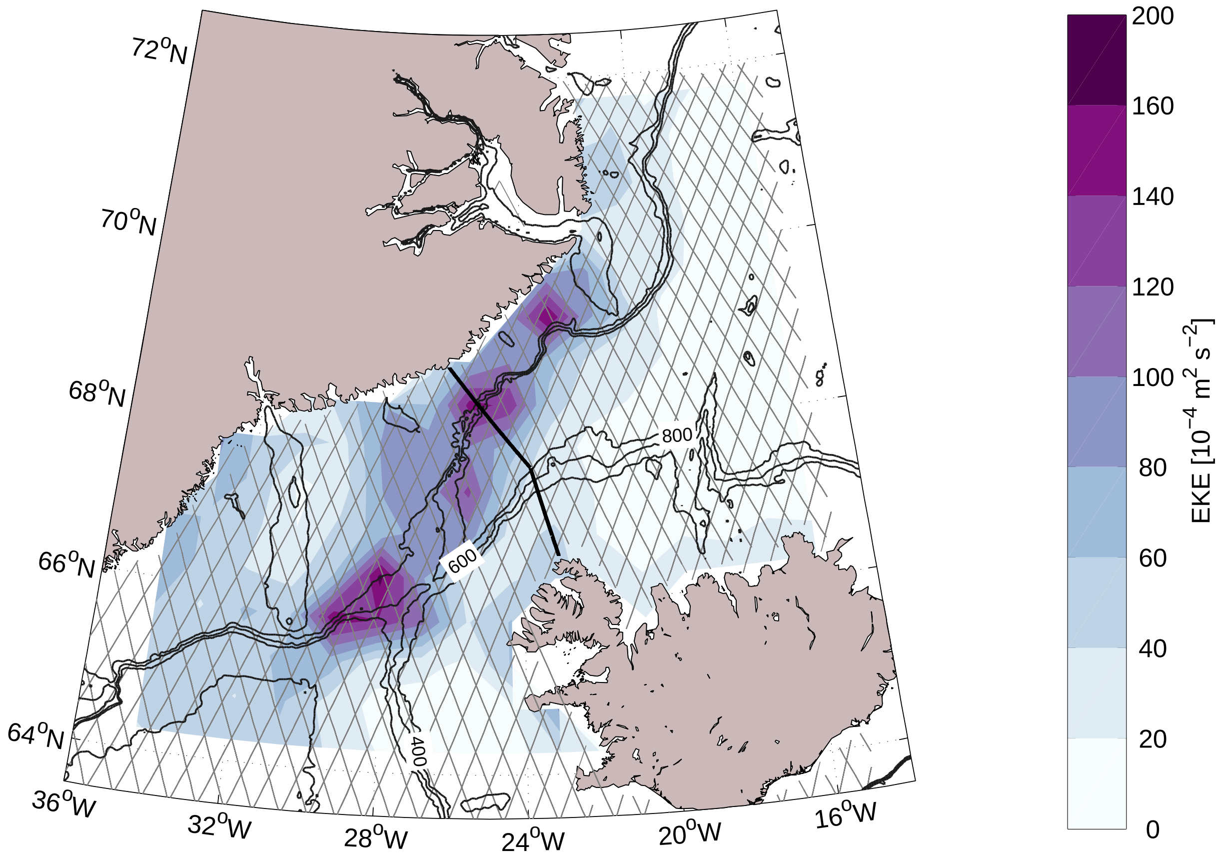

FIG. 9. Map of median surface EKE_{alt} within the region of Denmark Strait, obtained from along-track sea level anomaly data from Envisat for the months August-October 2002-2011. The Kögur section is marked by the black line. The thin gray lines indicate the 35 day repeat cycle of the Envisat satellite.

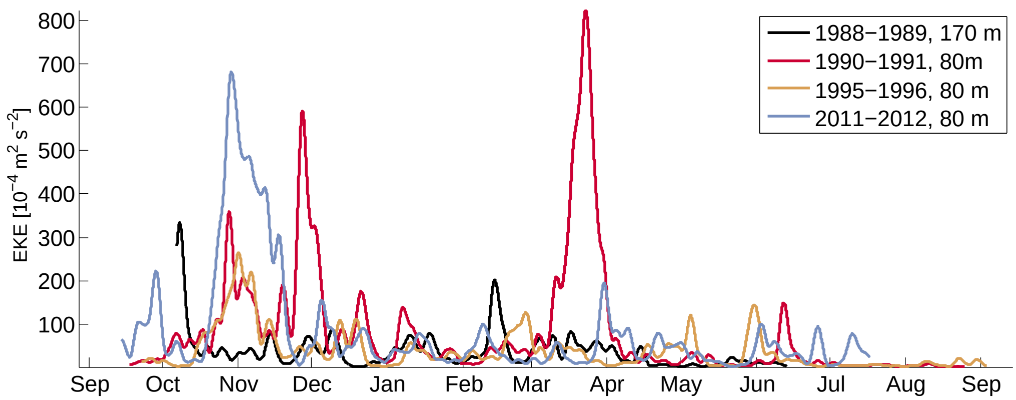

FIG. 10. Timeseries of band-pass filtered EKE$_{hist}$ estimates from four different years of moored observations. The historical data are from a position between KGA 11 and KGA 10 (see the Data and Methods section for details), and the timeseries from 2011-2012 is from the uppermost instrument at KGA 11.

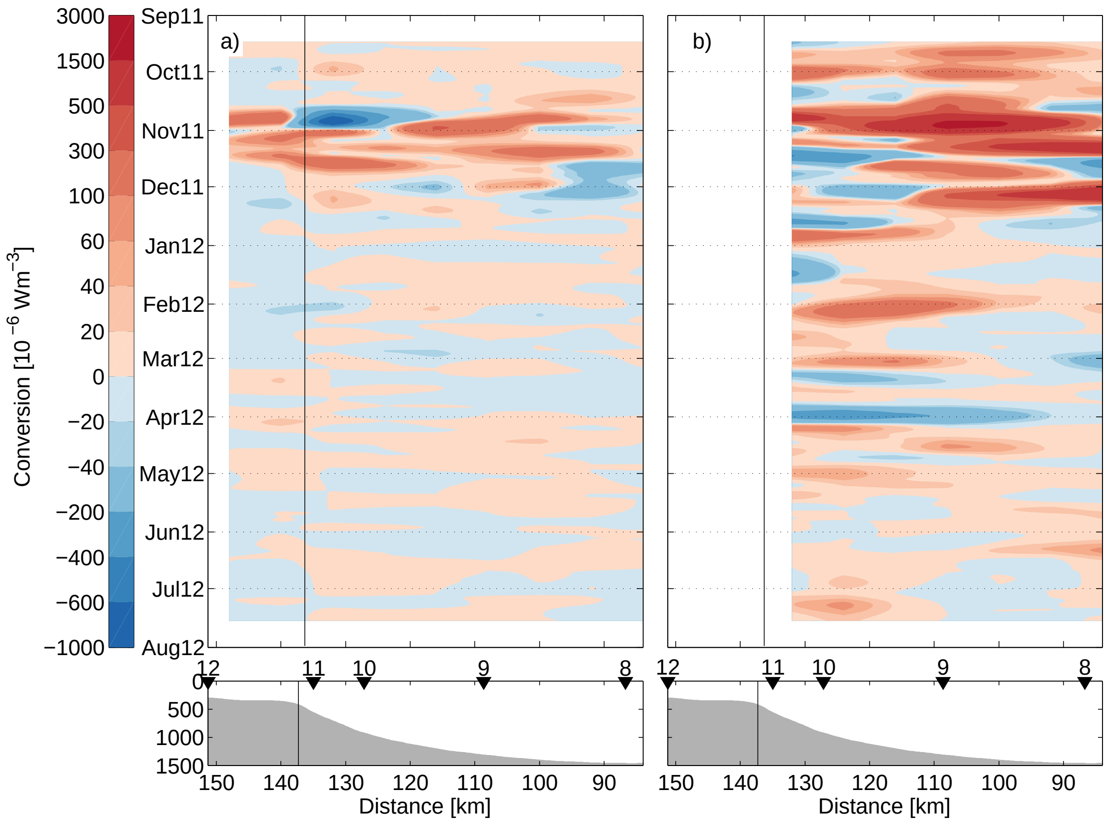

FIG. 11. Hovmöller diagrams of the barotropic conversion at 100 m (a) and the baroclinic conversion at 100 m (b). The lower panels show the bathymetry of the Kögur section. The black vertical lines mark the location of the shelfbreak. Positive conversions indicate extraction of energy from the mean flow to the eddies. Note the non-linear colorbar.

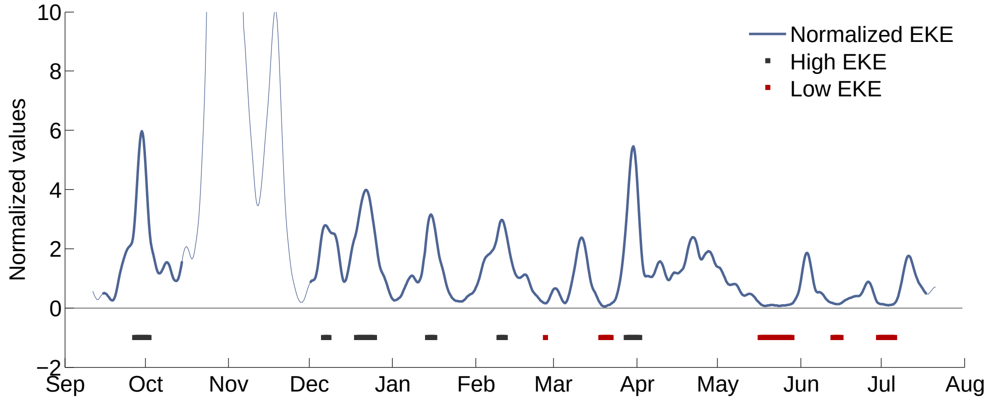

FIG. 12. Timeseries of normalized values of EKE_{moor} for the grid point closest to the shelfbreak at 100 m. Periods of high EKE_{moor} are marked with thick black lines. Periods of low EKE_{moor} are marked with thick red lines. These time steps form the composite means in Fig. 13. The period of the flow reversal during November, which was omitted from this analysis, is de-emphasized by thinner lines.

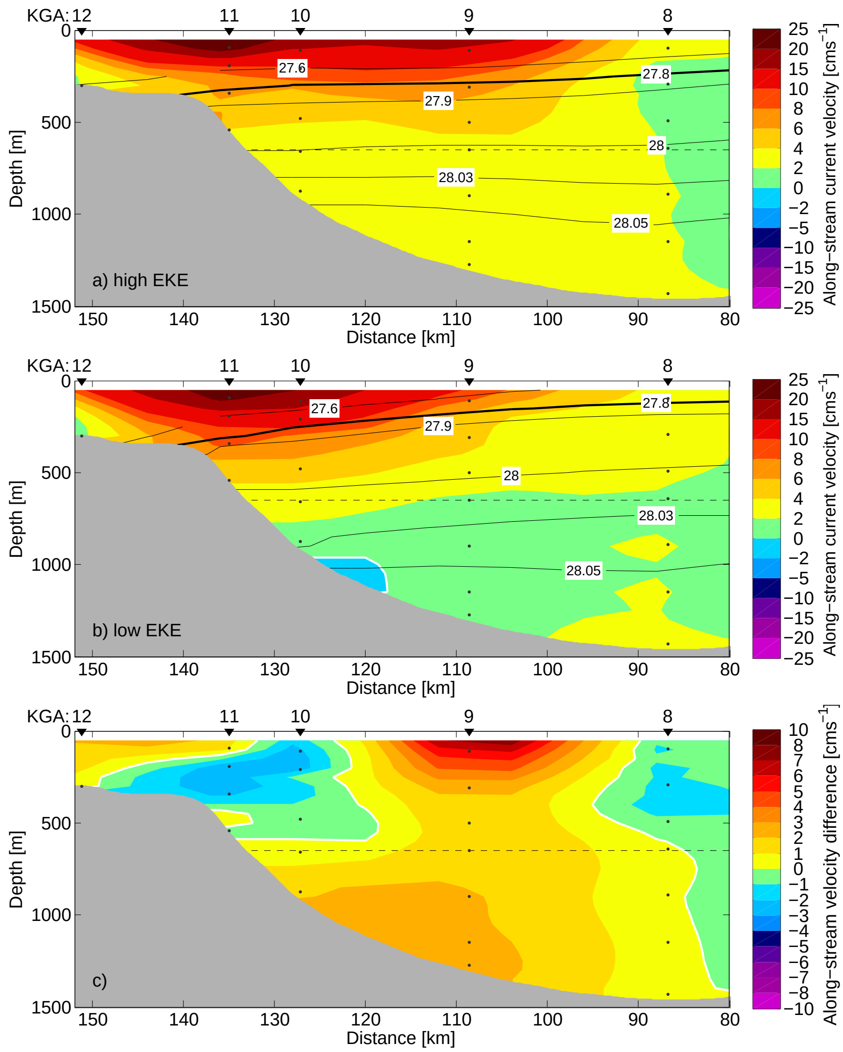

FIG. 13. Composite along-stream velocity at times of high EKE_{moor} (a) and low EKE_{moor} (b). (c) shows the difference between (a) and (b). The mooring locations are indicated on top of each section, and the instruments on each mooring by the black dots. The black contours are isopycnals, with the 27.8 kgm^{-3} isopycnal, highlighted in bold. The dashed line indicates the sill depth of Denmark Strait (650 m).